Hole doping and antiferromagnetic correlations above the Néel temperature of the topological semimetal $(Sr_{1-x}K_x)MnSb_2$

Yong Liu,[1,*] Farhan Islam,[1] Kevin W. Dennis,[1] Wei Tian,[2] Benjamin G. Ueland,[1,3]
Robert J. McQueeney,[1,3] and David Vaknin[1,3,†]

[1]*Division of Materials Sciences and Engineering, Ames Laboratory, U.S. DOE, Ames, Iowa 50011, USA*
[2]*Neutron Scattering Division, Oak Ridge National Laboratory, Oak Ridge, Tennessee 37831, USA*
[3]*Department of Physics and Astronomy, Iowa State University, Ames, Iowa 50011, USA*

Neutron diffraction and magnetic susceptibility studies of orthorhombic single crystal $(Sr_{0.97}K_{0.03})MnSb_2$ confirm the three-dimensional (3D) C-type antiferromagnetic (AFM) ordering of the Mn^{2+} moments at $T_N = 305 \pm 3$ K, which is slightly higher than that of the parent $SrMnSb_2$ with $T_N = 297 \pm 3$ K. Susceptibility measurements of the K-doped and parent crystals above T_N are characteristic of 2D AFM systems. This is consistent with high-temperature neutron diffraction of the parent compound that displays persisting 2D AFM correlations well above T_N to at least $\sim$560 K with no evidence of a ferromagnetic phase. Analysis of the de Haas–van Alphen magnetic oscillations of the K-doped crystal is consistent with hole doping.

I. INTRODUCTION

Magnetic semimetals $AMnPn_2$ (A = Sr, Ba, Ca; Pn = Sb and Bi) have attracted intense interest as they have the potential to exhibit topological electronic behaviors with the key signature of Dirac fermions based on first-principles calculation, angle-resolved photoelectron spectroscopy (ARPES), and quantum oscillations while also ordering antiferromagnetically [1–6]. These compounds consist of alternate stacking of Pn-Mn-Pn layers that are separated by A-Pn-A layers. In the A-Pn-A layer, Pn atoms are arranged in a square, or a distorted square lattice, that are predicted to host Dirac fermions with adequate spin-orbit coupling [1]. Indeed, theoretical calculations indicate that the electronic bands associated with the A-Pn-A layers are closer to the Fermi level than those arising from the Pn-Mn-Pn layers, and they display a linear energy-momentum dispersion similar to that in graphene, which is a key signature of the presence of Dirac fermions [2].

Dirac fermions in $AMnPn_2$ seem to display complex properties due to their interplay with the magnetism in the Mn planes leading to novel magnetotopological states. For example, it has been reported that Mn- and Sr-deficient $Sr_{1-y}Mn_{1-z}Sb_2$ with $y \sim 0.08$ and $z \sim 0.02$ is a Weyl semimetal that emerges by subjecting the Dirac fermions to a broken time-reversal symmetry via ferromagnetic (FM) ordering [7]. Specifically, this system is reported to undergo a FM transition below $T_C \simeq 565$ K, and an AFM transition below $T_N = 304$ K with a uniform canted moment that retains a weak net FM moment [7]. We note that we have recently found in

nearly stoichiometric $SrMn_2Sb_2$ that weak ferromagnetism is tied to impurities on the sample surface [8].

SbMnSb layers in $AMnSb_2$ (referred to as Mn-112 compounds) are common to a large family of layered pnictides such as AMn_2Pn_2 (referred to as Mn-122 compounds) and $RMnPnO$ (R = La, Ce, Pr, ...; 1111 compounds) that all settle into a G- or C-type AFM ground state corresponding to Néel or checkerboard spin ordering within the square layer and either AFM or FM coupling between layers, respectively [9–15]. It should be noted that the AFM is highly anisotropic as the in-plane exchange coupling among nearest-neighbor (NN) Mn^{2+} moments in the $MnPn$ planes (J_{2D}) is much stronger than the weaker interplane coupling J_i. As is usually observed in these and other layered systems [16,17], two-dimensional (2D) AFM correlations develop at temperatures that are significantly higher than the three-dimensional (3D) Néel temperature (T_N) [18]. Consequently, magnetic susceptibility versus temperature [$\chi(T)$] measurements show a very broad peak at temperatures that are much higher than T_N at an onset of emerging 2D AFM correlations [18]. In particular, for powder samples, $\chi(T)$ does not show strong features at T_N and only weak anomalies in $d\chi(T)/dT$ that reveal the transition to the 3D AFM phase.

Uniform moment canting in the AFM phase that produces a net FM moment, as has been reported for $Sr_{1-y}Mn_{1-z}Sb_2$ with $y \leqslant 0.1$ [7], is one way to break time-reversal symmetry. Another approach to achieving FM is inspired by recent studies that show that for hole doping, by substituting sufficient Ba with K (or Rb) as in $(Ba_{1-x}K_x)Mn_2As_2$, the localized antiferromagnetism on the Mn site is preserved and coexists with itinerant ferromagnetism associated with As bands [19,20]. Motivated by these reports, we studied similar substitutions in the Mn-112 systems that may provide an alternative route to inducing itinerant FM associated with the electronic band of Sb.

---

*Present address: Institute of High Energy Physics, Chinese Academy of Sciences, Beijing 100049, China and Dongguan Neutron Science Center, Dongguan 523803, China.
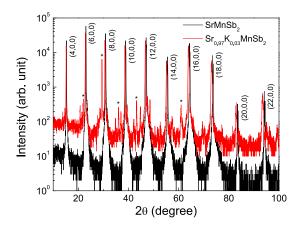†vaknin@ameslab.gov

FIG. 1. XRD patterns displaying the (H00) reflections up to the 22nd order for both crystals by using Cu $K\alpha$ radiation, shown on a logarithmic scale. Weak extra peaks for $(Sr_{0.97}K_{0.03})MnSb_2$ crystals, indicated by the asterisk, could not be matched with known impurity phases unequivocally.

Here, we report on the magnetic properties of single crystals of $SrMnSb_2$ and $(Sr_{0.97}K_{0.03})MnSb_2$ using the neutron diffraction technique in conjunction with various magnetization measurements. Although we find that the system can be hole-doped by K substitution of the Sr site, we also find that our approach to substitution is limited to values that are not sufficient to induce the desired FM state that is required for the Weyl state to exist.

II. EXPERIMENTAL DETAILS

Platelike $SrMnSb_2$ single crystals were grown by a self-flux method (more details can be found in Ref. [8]). K-substituted samples were prepared from a starting molar ratio of Sr : K : Mn : Sb $= 1 - x : 2x : 1 : 4$. The K content was doubled to avoid any loss during the crystal growth as it is an active and volatile element. We tried nominal $x = 0.1$, 0.2, and 0.5 compositions. For $x = 0.1$ and 0.2, the crystals were found to have an actual K concentration of $x = 0.03$, as determined by energy-dispersive x-ray spectroscopy (EDS) measurements. For the $x = 0.5$ growth, no crystals were obtained. This suggests that there is an extremely limited solubility of K in $SrMnSb_2$.

X-ray diffraction (XRD) measurements were performed on a Bruker D8 Advance Powder Diffractometer using Cu $K\alpha$ radiation. The single crystal was fixed to a sample stage by using clay. The surface of the platelike crystal was aligned with the surface of the edge of the sample stage by using a glass slide. Figure 1 shows XRD patterns of $SrMnSb_2$ and $(Sr_{0.97}K_{0.03})MnSb_2$ single crystals with their (H00) in the scattering plane. A set of (H00) diffraction peaks to the 22nd order is observed for both samples, from which we extract the lattice parameter a (which is perpendicular to the layers in the $Pmna$ space group), and they are determined as 23.051(5) and 23.27(5) Å for $SrMnSb_2$ and $(Sr_{0.97}K_{0.03})MnSb_2$, respectively. The slight increase in the a-spacing is expected as the atomic radius of K is slightly larger than that of Sr.

Magnetization measurements were performed using a Physical Property Measurement System (PPMS, Quantum

Design) equipped with a vibrating sample magnetometer (VSM). For the temperature-dependent magnetization measurements, the sample was cooled down to the desired temperature without a magnetic field or with an application of magnetic field, termed as ZFC and FC, respectively. The temperature-dependent magnetization data were then collected upon warming at 2 K/min and at a fixed field. The magnetic fields H were applied parallel to the plate ($\mathbf{H} \perp \mathbf{a}$) and perpendicular to the plate ($\mathbf{H} \| \mathbf{a}$).

Single-crystal neutron diffraction experiments were carried out on the HB-1A triple-axis spectrometer located at the High Flux Isotope Reactor at Oak Ridge National Laboratory. The HB-1A spectrometer operates with a fixed incident energy of $E_i = 14.64$ meV using a double pyrolytic graphite (PG) monochromator system. PG filters were placed before and after the second monochromator to reduce higher-order contamination in the incident beam achieving a ratio $\frac{I_\lambda}{2} : I_\lambda :\approx 10^{-4}$. The $(Sr_{0.97}K_{0.03})MnSb_2$ and $SrMnSb_2$ crystals were mounted with the (HK0) in the scattering plane (40′-40′-S-40′-80′ collimation). The $SrMnSb_2$ was also mounted with (0KL) in the scattering plane with a tighter resolution (40′-10′-S-10′-80′) to resolve the in-plane orthorhombic distortion. We note that some results on the parent $SrMnSb_2$ are reproduced from Ref. [8] for comparison with the K-doped sample, and some are new.

III. RESULTS AND DISCUSSION

The temperature dependence of the magnetic susceptibilities, $\chi \equiv M/H$, at an applied field of $H = 1$ T along the a direction of single crystals of $SrMnSb_2$ and $(Sr_{0.97}K_{0.03})MnSb_2$ are compared in Fig. 2(a). It is evident that the T_N for $(Sr_{0.97}K_{0.03})MnSb_2$ is slightly higher than $SrMnSb_2$. To better locate T_N, we identify a peak in $d\chi(T)/dT$ versus T as shown in the inset of Fig. 2(a) [18]. We note that our $\chi(T)$ measurements, and the neutron diffraction results of both crystals described below, are consistent with previous reports of a C-type AFM order [7].

Two features in the susceptibility indicate that both samples retain 2D AFM correlations at temperatures above T_N. First, there is only a subtle signature at T_N in the form of a small change in slope (T_N is confirmed by neutron diffraction data, as discussed below). Second, the susceptibility above T_N does not display the characteristic paramagnetic behavior, namely $\chi(T) \propto 1/T$ above the transition, but rather increases linearly with temperature above T_N [$\chi(T) \propto T$], as shown in Fig. 2(b). The increase in susceptibility above T_N and the broad peak are common signatures of 2D magnetic systems that develop large correlations prior to the 3D ordering, which can be driven by negligible interplane coupling. The inset in Fig. 2(b) shows the same measurements to higher temperatures including during the cooling of the crystals that clearly show the emergence of a chemical change, presumably at the surface, that generates ferromagnetic impurity. While cooling from the high temperature, a new superimposed FM component with $T_c \approx 560$ K is apparent. Figure 2(c) shows magnetization *versus* applied magnetic field (hysteresis curve applied in the bc plane) at room temperature of the same crystal on which the susceptibility shown in Fig. 2(b) was measured, indicating the emergence of the FM component
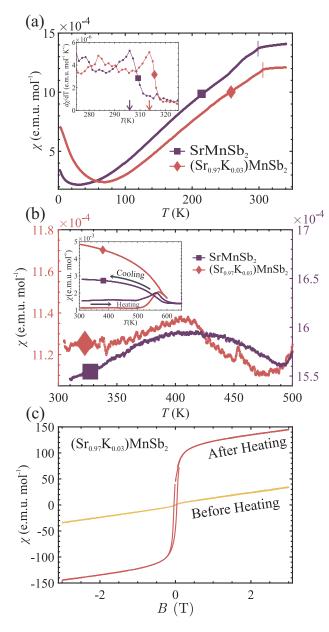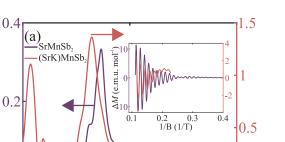
FIG. 2. (a) Zero-field-cooled (ZFC) magnetic susceptibility, $\chi \equiv M/H$, of single crystals SrMnSb$_2$ and (Sr$_{0.97}$K$_{0.03}$)MnSb$_2$ with applied magnetic field along the a-axis (χ_a) for SrMnSb$_2$ and (Sr$_{0.97}$K$_{0.03}$)MnSb$_2$ indicating a slight increase in T_N upon K-substitution. The inset shows $d\chi(T)/dT$ vs T with peaks at T_N that coincide with neutron diffraction extracted T_N's. The K-substituted single crystal exhibits a slightly higher T_N than the parent compound. (b) ZFC susceptibility at high temperatures (above T_N) for the parent and the doped crystals with magnetic field aligned in the bc plane. The increase in susceptibility above the T_N and the broad peak are common signatures of 2D magnetic systems that develop large correlations prior to the 3D ordering, which can be driven by negligible interplane coupling. The inset shows the same measurements to higher temperatures that indicate a chemical change, presumably at the surface, that generates ferromagnetic impurity. The inset also shows the susceptibility while cooling from the high temperature with a new superimposed FM component with $T_c \approx 560$ K. (c) Magnetization vs applied magnetic field at room temperature before and after heating the (Sr$_{0.97}$K$_{0.03}$)MnSb$_2$ sample used for the measurement shown in (b).
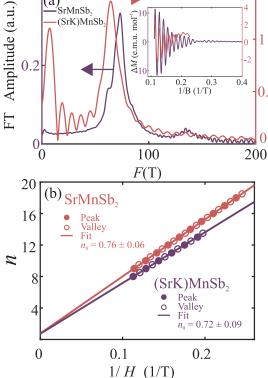

FIG. 3. (a) Comparison of the FT of the oscillating $M_a(B)$ for the parent SrMnSb$_2$ and the K-substituted (Sr$_{0.97}$K$_{0.03}$)MnSb$_2$. The inset shows $\Delta M_a(1/H)$ for both crystals as indicated. (b) Enumerating peak and valleys in (a) as a function of $1/H$ (assigning integers to minima). The intercepts at $n(1/H \rightarrow 0) = 0.76(6)$ and $0.72(9)$ for both crystals as indicated.

after heating the sample. Multiple cycles of heating/cooling the crystal show that the FM component does not increase after the second one (data not shown).

To further characterize the parent and K-doped crystals, we measured the magnetization versus applied magnetic field along a and in the bc plane [$M_a(H)$ and $M_{bc}(H)$]. Whereas $M_{bc}(H)$ exhibits a linear dependence on H as is usual for an applied field perpendicular to the moment direction in AFM crystals (not shown), the $M_a(H)$ exhibits strong de Haas–van Alphen (dHvA) oscillations. The inset in Fig. 3(a) shows the oscillating part of the magnetization versus $1/H$ after subtracting an analytical function $M_a(H) = c_1 \text{erf}(c_2 H) + c_3 H + c_4$ from raw data with adjusted parameters c_i. By performing a numerical Fourier transform (FT), we obtain the spectral FT signals shown in Fig. 3(a). The spectra shows similar features to those obtained in Refs. [7,8] with a prominent peak at 73.1(2) T and a second peak at 137.0(5) T, not quite at the second harmonic position. We note that for the K-substituted sample, the main peak shifts to lower fields from 73.1(2) T for the parent compound to 64(1) T. In addition, we consistently observe a low-frequency peak at $\sim$7.3 T, which can be an artifact due to the low quality of the signal and due to the cutoff at large $1/H$ (K-substituted crystals are much smaller than the parent ones).
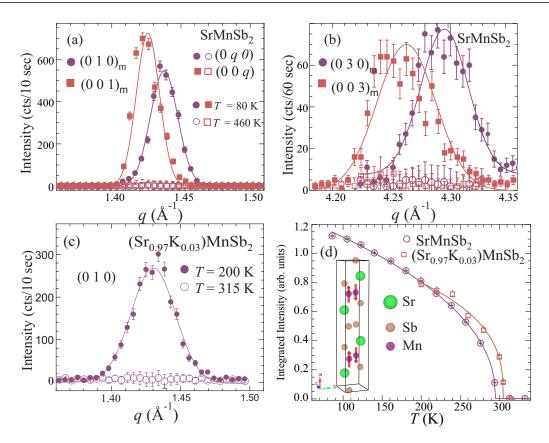
FIG. 4. Intensity of magnetic Bragg reflections (a) (010) and (001) and (b) (030) and (003) vs momentum transfer for the stoichiometric single crystal $SrMnSb_2$ below and above T_N. As is evident, the crystal is, to a large extent, not twinned. (c) The intensity of magnetic Bragg reflections (a) (010) for $(Sr_{0.97}K_{0.03})MnSb_2$ below and above T_N as indicated. (d) The intensities vs temperature of the magnetic (010) including a fit (solid line) to a power law $I \propto (1 - T/T_N)^{2\beta}$ yield $T_N = 297(2)$ and $305(4)$ K and $\beta = 0.227(2)$ and $0.173(3)$ for the pure and K-doped crystals [$(Sr_{0.97}K_{0.03})MnSb_2$], respectively. The inset illustrates atomic chemical and magnetic structure.

Figure 3(b) shows the enumeration of peaks and valleys of $\Delta M_a(1/H)$ by assigning integers to minima. The intercepts for both crystals are at $n(1/H \rightarrow 0) = 0.76(6)$ and $0.72(9)$ for the $SrMnSb_2$ and $(Sr_{0.97}K_{0.03})MnSb_2$, respectively. The value of the intercept relates to the Berry phase. It was reported that the intercept n is 0.55 in $Sr_{1-y}Mn_{1-z}Sb_2$ with $y \sim 0.08$ and $z \sim 0.02$ through an analysis of Shubnikov–de Haas (SdH) oscillation, close to the expected value of 0.55 for a 2D or quasi-2D system with relativistic fermions [7]. However, another transport analysis yields $n = 0.14$ for $SrMnSb_2$ with a relatively low saturated magnetization moment, which suggests trivial topology [21]. The hole doping does not affect the n value extracted from the analysis of dHvA oscillations, suggesting that both the parent and hole-doped compounds share similar topological characteristics, trivial or nontrivial. The intercept we observe in the dHvA oscillations [Fig. 3(b)], whether related to a nontrivial Berry phase or not, is still an open question.

Figures 4(a) and 4(b) show the intensities of the (010)/(001) and the (030)(003) AFM peaks, respectively, at 80 and 460 K for single crystal $SrMnSb_2$, and Fig. 4(c) shows the (010)/(001) AFM peaks for the K-substituted $(Sr_{0.97}K_{0.03})MnSb_2$. As shown, the distinct (unsplit) planar orthorhombic peaks indicate a single crystal with almost no detectable orthorhombic twinning. Figure 4(d) shows the intensity of the (010) magnetic peaks below and above T_N.

The magnetic peaks for both the parent and K-doped compounds are consistent with the magnetic structure previously reported [7]. The intensities versus temperature of the (010) magnetic Bragg reflections with fit (solid lines) to a power law $I \propto (1 - T/T_N)^{2\beta}$ yield $T_N = 297(2)$ and $305(4)$ K and $\beta = 0.227(2)$ and $0.173(3)$ for the pure and K-substituted crystals, respectively. The inset in (d) illustrates the chemical and magnetic structures. The increase in T_N for the K-substituted crystal is in agreement with the determination of T_N from the susceptibility measurements. Using a few magnetic and nuclear Bragg reflections, we estimate the average staggered magnetic moment per Mn^{2+} at 4.0(5) μ_B at 200 K for both samples.

An important finding in this study is the persistence of AFM correlations (likely quasielastic) as observed for the magnetic (010) reflection [Fig. 5(a)] at temperatures significantly higher than T_N. These observations point to 2D correlations in the MnPn planes that develop at temperatures well above T_N. Figure 5 shows the (010) AFM peak at 80 K along with quasielastic scattering at 313 and 481 K (note that the intensities above T_N are multiplied by a factor of 500). The peaks above T_N are much broader with a FWHM that sets an upper limit to the 2D correlations at $\sim$80 Å. The temperature dependence of the integrated intensity of the (010) peak as a function of temperature is shown in Fig. 5(b) over the extended temperature range (on a semilogarithmic
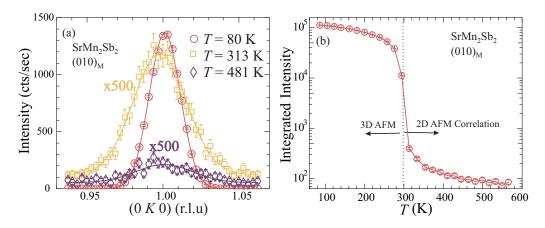
FIG. 5. (a) Magnetic Bragg reflection (010) at 80 K along with quasielastic scattering at 313 and 481 K (the intensities of peaks above T_N are multiplied by a factor of 500). The FWHM of the peaks above T_N suggests an upper limit for the average 2D correlations at 80 Å. (b) Temperature dependence of the integrated intensity of the (010) peak over the extended temperature range (on a semilogarithmic scale) showing the persistence of magnetic scattering to the highest temperature measured with no indication of a transition up to ~575 K.

scale) indicating the persistence of magnetic scattering to the highest temperature measured with no indication of a transition up to ~575 K. This 2D scattering has been observed before for other 2D systems, in particular for the the 1111 type AMnPnO systems with planes that are weakly coupled magnetically [12–15].

Our neutron diffraction and the temperature-dependent susceptibility results show that the nearly stoichiometric SrMnSb$_2$ and the K-doped compounds do not exhibit un-equivocal intrinsic spontaneous ferromagnetism. Given that the potential interest in the SrMnSb$_2$ is predicated on the development of a FM component in the bc plane, careful consideration must be given to the presence of FM impurities, which may be present in the as-grown samples or may develop at high-temperature conditions, such as those shown in Fig. 2(b) and those reported recently [8].

IV. SUMMARY

We report neutron diffraction and magnetization measurements of single-crystal (Sr$_{0.97}$K$_{0.03}$)MnSb$_2$ and compare them with those of the parent compound SrMnSb$_2$. Our synthesis efforts indicate a very low limit in the substitution of K for Sr on the order of a few percent. We confirm that the K-substituted compound undergoes a C-type AFM transition below $T_N = 305(3)$ K, which is slightly higher than that of the parent SrMnSb$_2$ for which $T_N = 297(3)$ K. Both the parent and the K-substituted crystals show features in the high-temperature susceptibility measurements (i.e., above T_N) that are characteristic of quasi-2D system evidence for 2D AFM correlations. Neutron diffraction measurements of the parent compound above T_N are consistent with the 2D correlations that clearly persist to almost twice T_N, and they also confirm

that the *Pnma* symmetry is preserved with no detectable evidence for a FM phase in the 80–600 K temperature range. The persistence of such 2D correlations to high temperatures is consistent with the layered structure, where magnetic Mn layers are well separated with interplanar coupling J_a that is much weaker than the intralayer exchange constants J_b or J_c, and consistent with spin-wave results of similar Mn layers in Mn-122 compounds. We caution that elevating the temperature of the crystals above ~500 K even under vacuum (~10^{-6} Torr), as in our susceptibility measurements, causes a slight chemical change (presumably at the surface) that creates a minute but detectable FM impurity phase with $T_C \approx 560$ K. Magnetization measurements up to 9 T show strong dHvA oscillations for the (Sr$_{0.97}$K$_{0.03}$)MnSb$_2$ crystal with Fourier transform at (FT[$M_a(1/H)$] $\simeq 64$ T) compared to that of the SrMnSb$_2$ at FT[$M_a(1/H)$] $= 73.1$ T. Whereas the K-substitution affects the electronic properties as observed in dHvA oscillations, the hole doping of the system does not induce the desired itinerant ferromagnetism necessary to break time-reversal symmetry. This may be due to the limited level of substitution of K for Sr in this system.

[1] M. A. Farhan, L. Geunsik, and S. Ji Hoon, *AE*MnSb$_2$(*AE* = Sr, Ba): A new class of Dirac materials, J. Phys.: Condens. Matter **26**, 042201 (2014).

[2] G. Lee, M. A. Farhan, J. S. Kim, and J. H. Shim, Anisotropic Dirac electronic structures of AMnBi$_2$ (A = Sr, Ca), Phys. Rev. B **87**, 245104 (2013).

[3] J. Park, G. Lee, F. Wolff-Fabris, Y. Y. Koh, M. J. Eom, Y. K. Kim, M. A. Farhan, Y. J. Jo, C. Kim, J. H. Shim, and J. S. Kim, Anisotropic Dirac Fermions in a Bi Square Net of $SrMnBi_2$, Phys. Rev. Lett. **107**, 126402 (2011).

[4] K. Wang, D. Graf, H. Lei, S. W. Tozer, and C. Petrovic, Quantum transport of two-dimensional Dirac fermions in $SrMnBi_2$, Phys. Rev. B **84**, 220401(R) (2011).

[5] K. Wang, D. Graf, H. Lei, S. W. Tozer, and C. Petrovic, Two-dimensional Dirac fermions and quantum magnetoresistance in $CaMnBi_2$, Phys. Rev. B **85**, 041101(R) (2012).

[6] K. Wang, L. Wang, and C. Petrovic, Large magnetothermopower effect in Dirac materials $(Sr/Ca)MnBi_2$, Appl. Phys. Lett. **100**, 112111 (2012).

[7] J. Y. Liu, J. Hu, Q. Zhang, D. Graf, H. B. Cao, S. M. A. Radmanesh, D. J. Adams, Y. L. Zhu, G. F. Cheng, X. Liu, W. A. Phelan, J. Wei, M. Jaime, F. Balakirev, D. A. Tennant, J. F. DiTusa, I. Chiorescu, L. Spinu, and Z. Q. Mao, A magnetic topological semimetal $Sr_{1-y}Mn_{1-z}Sb_2$ (y, $z < 0.1$), Nat. Mater. **16**, 905 (2017).

[8] Y. Liu, T. Ma, L. Zhou, W. E. Straszheim, F. Islam, B. A. Jensen, W. Tian, T. Heitmann, R. A. Rosenberg, J. M. Wilde, B. Li, A. Kreyssig, A. I. Goldman, B. G. Ueland, R. J. McQueeney, and D. Vaknin, Crystal growth, microstructure, and physical properties of $SrMnSb_2$, Phys. Rev. B **99**, 054435 (2019).

[9] J. An, A. S. Sefat, D. J. Singh, and M.-H. Du, Electronic structure and magnetism in $BaMn_2As_2$ and $BaMn_2Sb_2$, Phys. Rev. B **79**, 075120 (2009).

[10] Y. Singh, A. Ellern, and D. C. Johnston, Magnetic, transport, and thermal properties of single crystals of the layered arsenide $BaMn_2As_2$, Phys. Rev. B **79**, 094519 (2009).

[11] Y. Singh, M. A. Green, Q. Huang, A. Kreyssig, R. J. McQueeney, D. C. Johnston, and A. I. Goldman, Magnetic order in $BaMn_2As_2$ from neutron diffraction measurements, Phys. Rev. B **80**, 100403(R) (2009).

[12] Q. Zhang, W. Tian, S. G. Peterson, K. W. Dennis, and D. Vaknin, Spin reorientation and Ce-Mn coupling in antiferromagnetic oxypnictide $CeMnAsO$, Phys. Rev. B **91**, 064418 (2015).

[13] M. A. McGuire and V. O. Garlea, Short- and long-range magnetic order in $LaMnAsO$, Phys. Rev. B **93**, 054404 (2016).

[14] Q. Zhang, C. M. N. Kumar, W. Tian, K. W. Dennis, A. I. Goldman, and D. Vaknin, Structure and magnetic properties of $LnMnSbO$ ($Ln=$ La and Ce), Phys. Rev. B **93**, 094413 (2016).

[15] Y. Liu, W. E. Straszheim, P. Das, F. Islam, T. W. Heitmann, R. J. McQueeney, and D. Vaknin, Synthesis and Characterization of Ca-Doped $LaMnAsO$, Phys. Rev. Materials **2**, 054410 (2018).

[16] N. S. Sangeetha, A. Pandey, Z. A. Benson, and D. C. Johnston, Strong magnetic correlations to 900 K in single crystals of the trigonal antiferromagnetic insulators $SrMn_2As_2$ and $CaMn_2As_2$, Phys. Rev. B **94**, 094417 (2016).

[17] D. Vaknin, E. Caignol, P. K. Davies, J. E. Fischer, D. C. Johnston, and D. P. Goshorn, Antiferromagnetism in $(Ca_{0.85}Sr_{0.15})CuO_2$, the parent of the cuprate family of superconducting compounds, Phys. Rev. B **39**, 9122 (1989).

[18] J. Curély and J. Rouch, Thermodynamics of the 2D-Heisenberg classical square lattice Part III. Study of the static susceptibility behaviours, Phys. B **254**, 298 (1998).

[19] A. Pandey, B. G. Ueland, S. Yeninas, A. Kreyssig, A. Sapkota, Y. Zhao, J. S. Helton, J. W. Lynn, R. J. McQueeney, Y. Furukawa, A. I. Goldman, and D. C. Johnston, Coexistence of Half-Metallic Itinerant Ferromagnetism with Local-Moment Antiferromagnetism in $Ba_{0.6}K_{0.4}Mn_2As_2$, Phys. Rev. Lett. **111**, 047001 (2013).

[20] B. G. Ueland, *et al.*, Itinerant Ferromagnetism in the As-4p Conduction Band of $Ba_{0.6}K_{0.4}Mn_2As_2$ Identified by x-Ray Magnetic Circular Dichroism, Phys. Rev. Lett. **114**, 217001 (2015).

[21] S. V. Ramankutty, J. Henke, A. Schiphorst, R. Nutakki, S. Bron, G. Araizi-Kanoutas, S. K. Mishra, L. Li, Y. Huang, T. K. Kim, M. Hoesch, C. Schlueter, T.-L. Lee, A. Visser, Z. Zhong, J. van Wezel, E. van Heumen, and M. S. Golden, Electronic structure of the candidate 2D Dirac semimetal $SrMnSb_2$: A combined experimental and theoretical study, Sci. Post. Phys. **4**, 010 (2018).